GeoScienceWorld
Lithosphere
Volume 2024, Article ID lithosphere_2023_288, 12 pages
https://doi.org/10.2113/2024/lithosphere_2023_288

Lithosphere

*Research Article*

# Investigating the Mechanism of Strong Roof Weighting and Support Resistance Near Main Withdrawal Roadway in Large-Height Mining Face

**Junwu Du**[1,2,3] **and Qingxiang Huang**[1,3]

[1]*College of Energy Engineering, Xi'an University of Science and Technology, Xi'an, 710054, China*
[2]*State Key Laboratory for Fine Exploration and Intelligent Development of Coal Resources, Xuzhou, 221116, China*
[3]*Key Laboratory of Western Mine Exploitation and Hazard Prevention, Ministry of Education, Xi'an, 710054, China*

Correspondence should be addressed to Junwu Du; dujw@xust.edu.cn and Qingxiang Huang; huangqx@xust.edu.cn

Received 25 September 2023; Accepted 19 January 2024; Published 16 February 2024

Academic Editor: Yuqi Wu



Aiming at investigating the strong roof weighting when the large height mining face is nearing the main withdrawal roadway, the 52,304 working face (WF) nearly through the main withdrawal roadway mining in a colliery of Shendong coalfield was taken as the research background. The ground pressure, roof structure, and superposition effect of stress in the last mining stage were studied by field measurement, physical simulation, and numerical calculations. The obtained results demonstrated that the main roof formed the "long step voussoir beam" structure under the influence of the main withdrawal roadway. The superposition effect of the front abutment pressure of the WF and the concentrated stress of the main withdrawal roadway caused the stress asymmetrical distribution on the two sides -level hard rock straof the main withdrawal roadway, and the stability of the pillar on the mining side decreases. The initial average periodic weighting interval was 20.7 m. While the WF approaches the main withdrawal roadway, the pillar near the WF of the main withdrawal roadway collapsed, the main roof was broken ahead of the WF, and the actual roof control distance of support and the periodic weighting interval increased by 2.56 and 1.26 times the normal state, respectively. Consequently, the "static load" of the immediate roof and the "dynamic load" of the sliding unsteadiness of the long step voussoir beam increased. The structural model of the "long step voussoir beam" under the superposition of "static and dynamic load" was established concerning those results, and an expression was proposed to compute the support resistance. Meanwhile, the mechanism of strong roof weighting was revealed when the WF was nearly through the main withdrawal roadway. The research conclusion is expected to provide a guideline for the safe withdrawal of the large-height mining faces under similar conditions.

## 1. Introduction

To increase the withdrawal speed and yield efficacy of the working face (WF) and avoid the tense connection between face mining and entry driving, predriving double withdrawal roadway is widely used in coal mines to reinforce the withdrawal operation [1]. In this scheme, the main and auxiliary withdrawal roadways are advance driven at the stop-mining line of the WF. After the primary withdrawal roadway is connected with the WF, the reinforcements are withdrawn through the connecting entry between the primary and secondary withdrawal roadways. Consequently, the withdrawal speed of the WF increases 3–5 times compared with the traditional methods, thereby increasing the production rate and improving the mining efficiency [2, 3]. Although this method has remarkable advantages, it has some shortcomings, including low mining speed in the last mining stage, concentrated mining-induced stress field, and high roof pressure [4]. More specifically, the superposition effect of the lateral and front abutment pressure of the main withdrawal roadway and the WF near the main withdrawal roadway is significant, and

| Serial number | Rock strata | Bar graph | Thickness (m) | Cumulative depth (m) |
|---|---|---|---|---|
| 1 | Siltstone | | 9.16 | 113.01 |
| 2 | Medium sandstone | | 1.92 | 114.93 |
| 3 | Fine sandstone | | 4.92 | 119.85 |
| 4 | Siltstone | | 4.17 | 124.02 |
| 5 | Medium sandstone | | 1.50 | 125.52 |
| 6 | Siltstone | | 2.40 | 127.92 |
| 7 | Fine sandstone | | 3.84 | 131.76 |
| 8 | Coal line | | 0.30 | 132.06 |
| 9 | Mudstone | | 1.55 | 133.61 |
| 10 | Medium sandstone | | 1.25 | 134.86 |
| 11 | Fine sandstone | | 2.69 | 137.55 |
| 12 | Mudstone | | 8.03 | 145.58 |
| 13 | Medium sandstone | | 12.73 | 158.31 |
| 14 | Mudstone | | 0.76 | 159.07 |
| 15 | Coal line | | 0.50 | 159.57 |
| 16 | Kernstone | | 7.76 | 167.33 |
| 17 | Medium sandstone | | 3.89 | 171.22 |
| 18 | Fine sandstone | | 4.17 | 175.93 |
| 19 | Mudstone | | 0.69 | 176.62 |
| 20 | Fine sandstone | | 1.03 | 177.65 |
| 21 | Mudstone | | 0.31 | 177.96 |
| 22 | 5-2 coal seam | | 7.15 | 185.11 |
| 23 | Siltstone | | 4.10 | 189.21 |

Figure 1: The D168 rock strata bar graph of the WF.

the roof control distance of the WF is large. Consequently, roof fall and support crushing are prone to happen, which seriously reduces the withdrawal speed and safe operation of the WF.

Recently, several articles have been published on stopping mining and waiting for roof weighting, reinforcing the withdrawal roadway, and optimizing the width of the coal pillar of the withdrawal roadways. In this regard, Zheng et al. [5] focused on the influence of the mining speed on the periodic weighting interval distance. Han et al. [6] clarified the influence of advance speed on the overburden movement law of a fully mechanized longwall face. Wang et al. [7, 8] revealed the effect of stopping mining and waiting for roof weighting in the final mining stage on the mining efficiency. Moreover, Yang et al. [9] applied traditional methods and studied the optimal stopping mining position and the waiting roof weight. Yang et al. [10] proposed an innovative method to change the position of periodic weighting by reducing the continuous length of periodic weighting and realizing the safe withdrawal of WF. Ma et al. [11] used organic grouting materials to strengthen the mining side pillar of the main withdrawal roadway and avoid rib spalling and roof collapse of the WF near the main withdrawal roadway. Gao [12] used the Malisan pregrouting to reinforce the coal wall and significantly reduced the rib spalling in the last mining stage of grand mining height longwall faces. Yao et al. [13] applied large aperture hydraulic presplitting technology to change roof behavior and reduce the dynamic load of support in the final mining stage. Lou et al. [14] used physical simulation to reveal the evolution law of mining-induced stress field in longwall WF. Gu et al. [15–17] established the roof structure mechanical model to determine the coal pillar load and width of the withdrawal roadway in the last mining stage of the longwall face. Wang et al. [18] applied the cooperative operation technology of WF mining and studied withdrawal analytically. Lv [19] established a mechanical model and characterized the pillar stress variation of coal pillars in the last mining gallery of the WF. Zhang et al. [20, 21] summarized the evaluation methods for coal pillar failure and instability and studied the overburden migration monitoring system of shallow-buried high-intensity mining. Li et al. [22] studied the failure mechanism and control measures of composite roof roadways through practical cases. Gao et al. [23] studied the effect of ground pressure by subjecting high-level hard rock strata. Furthermore, Huang et al. [24–26] established the equivalent immediate roof of a large-height mining longwall face, the height step voussoir beam structure of the roof, and proposed a modified method to evaluate the support working resistance of large-height mining longwall face.

In summary, the performed investigations in this area are mainly focused on the superposition effect of pillar stress and pillar stability in the last mining stage. It was found that strong roof weighting mainly originates from the stability evolution of roof structure. Considering roof

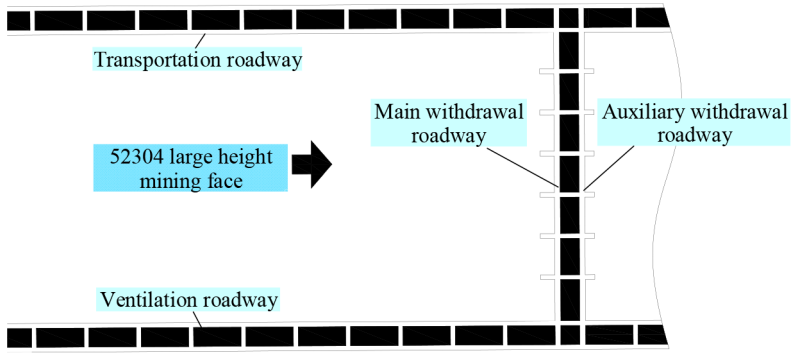


Figure 2: The plane layout of the WF in the last mining stage.

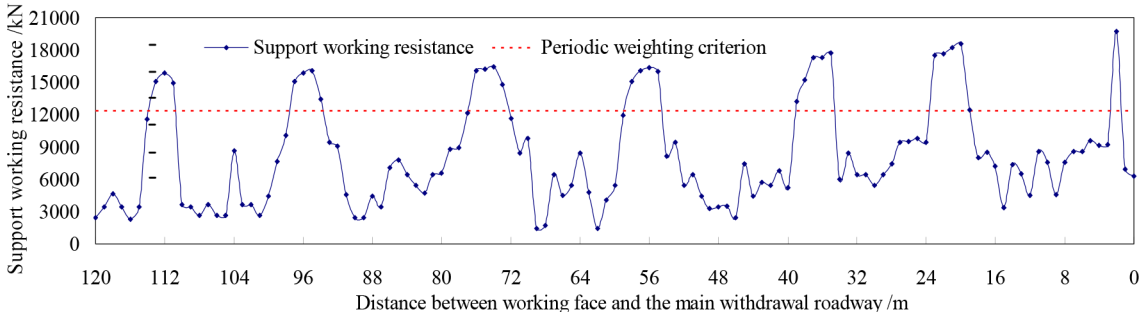


Figure 3: Support working resistance change curves.

collapse accidents and support crushing in the final mining of 52,304 large-height mining longwall faces, field measurements, physical simulation, numerical calculations, and mechanical analyses have been carried out to study the strong roof weighting mechanism.

This article was intended to establish a structural model of a "long step voussoir beam" subjected to "static loads" and "dynamic loads" and reveal the mechanism of roof fall and support crushing in the final mining of large-height mining longwall face.

## 2. Field Measurements Analyses of Ground Pressure in the Last Mining Stage of the WF

*2.1. General Conditions.* The 52304-WF (ZY16800/32/70D, Zhengzhou Coal Mining Machinery Group Co., China, hereafter called the WF) is an automatic hydraulic-powered support longwall face having a grand mining height and a panel of 301 m wide and 4548 m long, which mines $5^{-2}$ coal seam with a buried depth of 172 m. The mining height in the final stage is about 6.0 m, and the roof management is described as a fully caving method. The width, maximum roof control distance, and rated working resistance of the support are 2.05 m, 4.5 m, and 16,800 kN, respectively. The pillar width between the main and auxiliary withdrawal roadways is 20 m.

The bedrock of the studied area mainly consists of siltstone, fine sandstone, and medium sandstone, which belongs to the hard-to-cave roof. The D168 drill bar chart of the 52304-WF and the plane layout of the final mining stage are shown in Figures 1 and 2, respectively.

*2.2. Field Measurement Analysis of Ground Pressure in the Last Mining Stage.* In the present study, 150 PM32 lectro-hydraulic control systems from Zhengzhou Coal Mining Machinery Group Co. (China) were used on each hydraulic-powered support to survey the working resistance. Then the obtained data from five representative supports (supports 60, 70, 80, 90, and 100) were analyzed, and the distribution of support resistance within 120 m of the WF was obtained. Figure 3 indicates that the initial average periodic weighting interval in the final mining stage was 19.8 m, and the average working resistance during periodic weighting was 17,537 kN. It is observed that as the length between the WF and the primary withdrawal roadway increased, the corresponding maximum support working resistance increased continuously. Moreover, as the WF approached the main withdrawal roadway, the opening rate of the support safety valve reached 62% and the drop-out value of the hydraulic prop was 50–200 mm. The working resistance reached 19,720 kN in an instant, the roof fell, and the support crushed.

## 3. Physical Simulation in the Last Mining Stage

### 3.1. Design of Physical Model

*3.1.1. Determination of the Proportion of Physically Similar Materials.* According to the geological report (revised) of

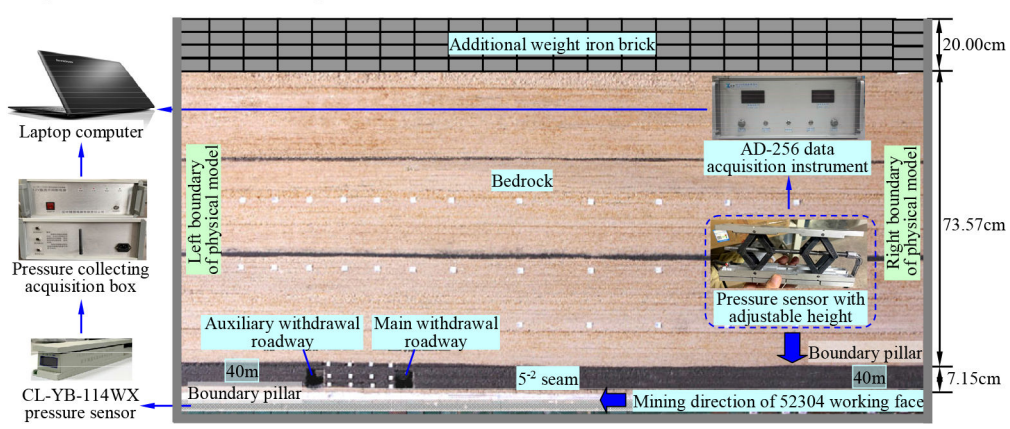


Figure 4: The physical model and monitoring scheme.

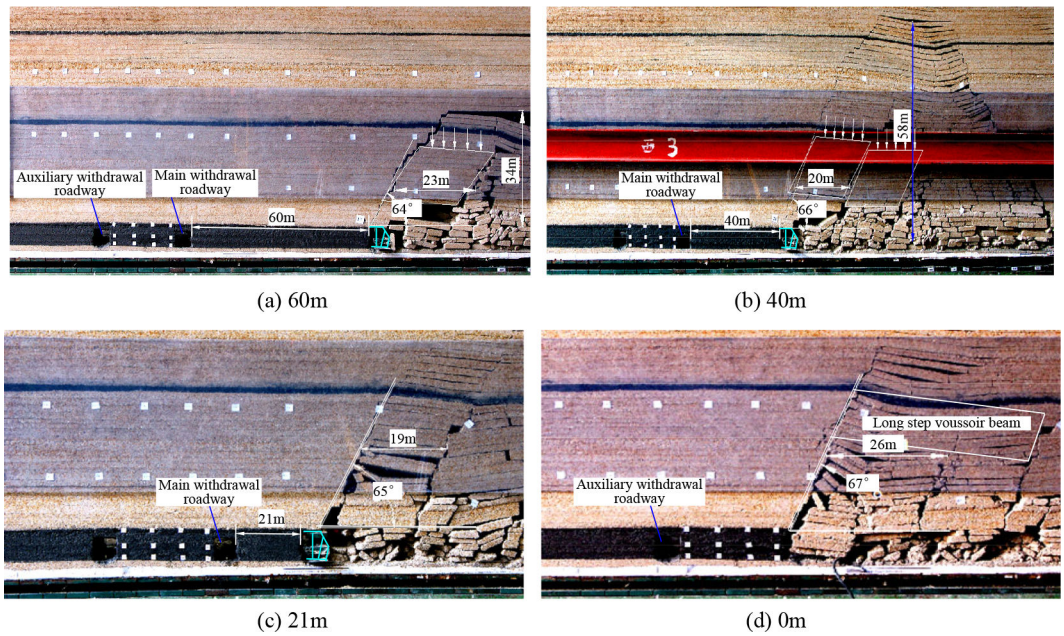


Figure 5: Simulation of the final mining stage at different distances from the WF to the main withdrawal roadway.

Daliuta Coal Mine and the geological data of D168 drilling core, the physical and mechanical parameters of the coal and rock of 52304-WF are shown in Table 1.

Aiming at revealing the roof weighting evolution and overburden structure characteristics in the last mining stage, its middle section was simulated. To this end, similarity parameters were set considering the physical and mechanical characteristics of overburden in the WF. The length and width of the physical model are 3.0 and 0.2 m, respectively, and its similarity constants are as follows:

Geometric similarity constant: $\alpha_l = \frac{l_m}{l_p} = \frac{1}{100}$

Gravitational similarity constant: $\alpha_\gamma = \frac{\gamma_m}{\gamma_p} = \frac{2}{3}$

Similarity constant of gravitational acceleration: $\alpha_g = \frac{g_m}{g_p} = \frac{1}{1}$

Time similarity constant: $\alpha_t = \frac{t_m}{t_p} = \sqrt{\alpha_l} = \frac{1}{10}$

Velocity similarity constant: $\alpha_v = \frac{v_m}{v_p} = \sqrt{\alpha_l} = \frac{1}{10}$

Displacement similarity constant: $\alpha_s = \alpha_l = \frac{1}{100}$

Similar conditions such as rock strength, elastic modulus, and bonding force: $\alpha_R = \alpha_E = \alpha_C = \alpha_l\alpha_\gamma = \frac{1}{150}$

Similarity constant of internal friction angle: $\alpha_\varphi = \frac{R_m}{R_p} = \frac{1}{1}$

Acting force similarity constant: $\alpha_f = \frac{f_m}{f_p} = \alpha_g\alpha_\gamma\alpha_l^3 = \frac{2}{3} \times 10^{-6}$ where the subscript $m$ represents the physical model, and the subscript $l$ represents the engineering prototype.

Table 1: Physical and mechanical properties of coal and strata.

| Strata number | Rock strata | Bulk density (MN/m$^3$) | Compressive strength (MPa) | Elastic modulus (MPa) | Cohesion (MPa) | Poisson's ratio |
|---|---|---|---|---|---|---|
| 1 | Siltstone | 24.6 | 36.5 | 2780 | 1.90 | 0.30 |
| 2 | Medium sandstone | 23.6 | 45.3 | 4599 | 2.80 | 0.29 |
| 3 | Fine sandstone | 22.8 | 25.2 | 9530 | 1.20 | 0.27 |
| 4 | Siltstone | 24.2 | 41.1 | 6050 | 1.65 | 0.32 |
| 5 | Medium sandstone | 23.4 | 48.3 | 7949 | 1.70 | 0.28 |
| 6 | Siltstone | 23.9 | 20.5 | 8350 | 0.15 | 0.34 |
| 7 | Fine sandstone | 22.7 | 27.6 | 6258 | 2.50 | 0.29 |
| 8 | Coal seam | 14.2 | 15.7 | 1450 | 1.30 | 0.28 |
| 9 | Mudstone | 25.6 | 26.8 | 8789 | 2.38 | 0.28 |
| 10 | Medium sandstone | 23.3 | 40.6 | 9949 | 1.50 | 0.28 |
| 11 | Fine sandstone | 23.4 | 38.5 | 10,629 | 1.88 | 0.27 |
| 12 | Mudstone | 24.7 | 41.2 | 8640 | 2.76 | 0.35 |
| 13 | Medium sandstone | 23.3 | 42.6 | 9949 | 2.50 | 0.38 |
| 14 | Mudstone | 23.9 | 35.2 | 9450 | 1.65 | 0.23 |
| 15 | Coal seam | 12.5 | 13.2 | 1700 | 1.23 | 0.23 |
| 16 | Kernstone | 24.2 | 26.8 | 8789 | 2.10 | 0.21 |
| 17 | Medium sandstone | 23.4 | 40.6 | 9949 | 1.87 | 0.30 |
| 18 | Fine sandstone | 24.3 | 26.8 | 8789 | 1.45 | 0.22 |
| 19 | Mudstone | 22.7 | 40.6 | 7949 | 1.35 | 0.28 |
| 20 | Fine sandstone | 23.9 | 26.8 | 8889 | 1.85 | 0.31 |
| 21 | Mudstone | 21.3 | 28.6 | 10,049 | 1.97 | 0.25 |
| 22 | 5–2 coal seam | 13.6 | 16.8 | 1890 | 1.38 | 0.28 |
| 23 | Siltstone | 25.7 | 26.8 | 7500 | 2.32 | 0.34 |

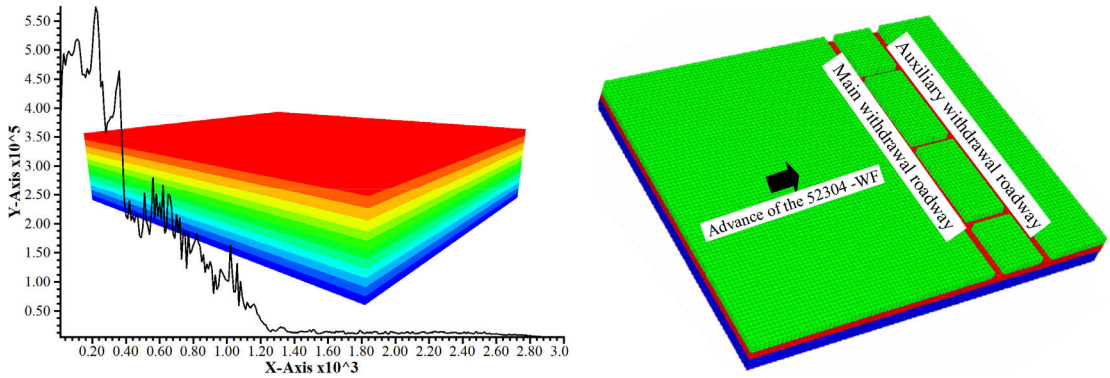


(a)Stress equilibrium curve (b)Simulation Scheme

Figure 6: The calculation model.

Based on the physical and mechanical parameters of D168 drilling core and the similarity constants of the physical model, the physical simulation materials ratio is calculated as shown in Table 2. In the calculation, the density of sand is taken as 1600 kg/m$^3$, the density of gypsum is taken as 2300 kg/m$^3$, the density of fly ash is taken as 1300 kg/m$^3$, and the density of lithopone is taken as 1400 kg/m$^3$.

Since the average burial depth of 52304-WF is 172 m, the physical model is paved with some rock strata, and the rest overburden is simulated by iron brick equivalent. Therefore, the coal seam, thickness of the bedrock, and additional iron brick layers of the physical model were set to 7.15, 73.57, and 20.0 cm, respectively.

Table 2: Ratio of component materials in simulated materials.

| Strata number | Rock strata | Thickness (cm) | Component material | Material used in each stratum (kg/cm) | | | |
|---|---|---|---|---|---|---|---|
| | | | | Sand | Gypsum | Lithopone | Fly ash |
| 1 | Siltstone | 9.16 | 837 | 8.53 | 0.46 | 0.65 | |
| 2 | Medium sandstone | 1.92 | 737 | 8.40 | 0.52 | 0.74 | |
| 3 | Fine sandstone | 4.92 | 828 | 8.53 | 0.31 | 0.75 | |
| 4 | Siltstone | 4.17 | 728 | 8.40 | 0.35 | 0.84 | |
| 5 | Medium sandstone | 1.50 | 846 | 8.53 | 0.61 | 0.56 | |
| 6 | Siltstone | 2.40 | 837 | 8.53 | 0.46 | 0.65 | |
| 7 | Fine sandstone | 3.84 | 946 | 8.64 | 0.55 | 0.50 | |
| 8 | Coal seam | 0.30 | 20:20:1:5 | 4.17 | 0.30 | 0.91 | 3.39 |
| 9 | Mudstone | 1.55 | 828 | 8.53 | 0.31 | 0.75 | |
| 10 | Medium sandstone | 1.25 | 728 | 8.40 | 0.35 | 0.84 | |
| 11 | Fine sandstone | 2.69 | 737 | 8.40 | 0.52 | 0.74 | |
| 12 | Mudstone | 8.03 | 828 | 8.53 | 0.31 | 0.75 | |
| 13 | Medium sandstone | 12.73 | 746 | 8.40 | 0.69 | 0.63 | |
| 14 | Mudstone | 0.76 | 837 | 8.53 | 0.46 | 0.65 | |
| 15 | Coal seam | 0.50 | 20:20:1:5 | 4.17 | 0.30 | 0.91 | 3.39 |
| 16 | Kernstone | 7.76 | 828 | 8.53 | 0.31 | 0.75 | |
| 17 | Medium sandstone | 3.89 | 737 | 8.40 | 0.52 | 0.74 | |
| 18 | Fine sandstone | 4.17 | 828 | 8.53 | 0.31 | 0.75 | |
| 19 | Mudstone | 0.69 | 728 | 8.40 | 0.35 | 0.84 | |
| 20 | Fine sandstone | 1.03 | 837 | 8.53 | 0.46 | 0.65 | |
| 21 | Mudstone | 0.31 | 828 | 8.53 | 0.31 | 0.75 | |
| 22 | 5–2 coal seam | 7.15 | 20:20:1:5 | 4.17 | 0.30 | 0.91 | 3.39 |
| 23 | Siltstone | 4.10 | 828 | 8.53 | 0.31 | 0.75 | |

*3.1.2. Physical Model Stress Monitoring Equipment and Solutions.* In the physical model, the sixty pressure sensors (CL-YB-114WX, Hanzhong Jingce Electrical Appliance Co., Ltd, China) and the pressure sensor with adjustable height (Independent R&D and production) were adopted to survey the front abutment pressure and the support working resistance of the WF. During 52304-WF mining, the experimental data of the front abutment pressure and the support working resistance are recorded.

In addition, to eliminate the left and right boundary effects of the model, 40 m wide boundary coal pillars were left on both sides of the physical model. Before mining, the main and auxiliary withdrawal roadways were excavated at the model's left side, with a width of 5.0 cm each. The physical model and monitoring scheme are shown in Figure 4.

*3.2. Roof Caving and Ground Pressure in the Last Mining Gallery.* Based on the performed simulations, the predominant features when the 52304-WF in the last mining stage were as follows (Figure 5).

*3.2.1. Roof Caving and Roof Structural Characteristics*

The minimum, maximum, and average caving angles on the coal wall side of the WF were 64°, 67°, and 65°, respectively. Meanwhile, the rotation angle of the main roof key blocks was about 5°. As the WF approached the primary withdrawal roadway, the main roof caved ahead of the WF, and the "long step voussoir beam" slid and lost stability.

*3.2.2. Roof Weighting Appearance.* It is found that 60.0–21.0 m distant from the primary withdrawal roadway, the periodic weighting interval was decreased from 23.0 to 19.0 m, while the simulated support working resistance was increased from 17,320 to 17,850 kN. It should be indicated that the initial average periodic weighting interval of the WF and the average working resistance of the reinforcement were 20.7 m and 17,540 kN, respectively, which fit with the field measurement data.

In the vicinity of the main withdrawal roadway, the side coal pillar collapsed with the main roof caving ahead of the WF. Compared with the normal case, this phenomenon increased the actual roof control distance of the support by 2.56 times and the periodic weighting interval by 1.26 times. Meanwhile, there was strong

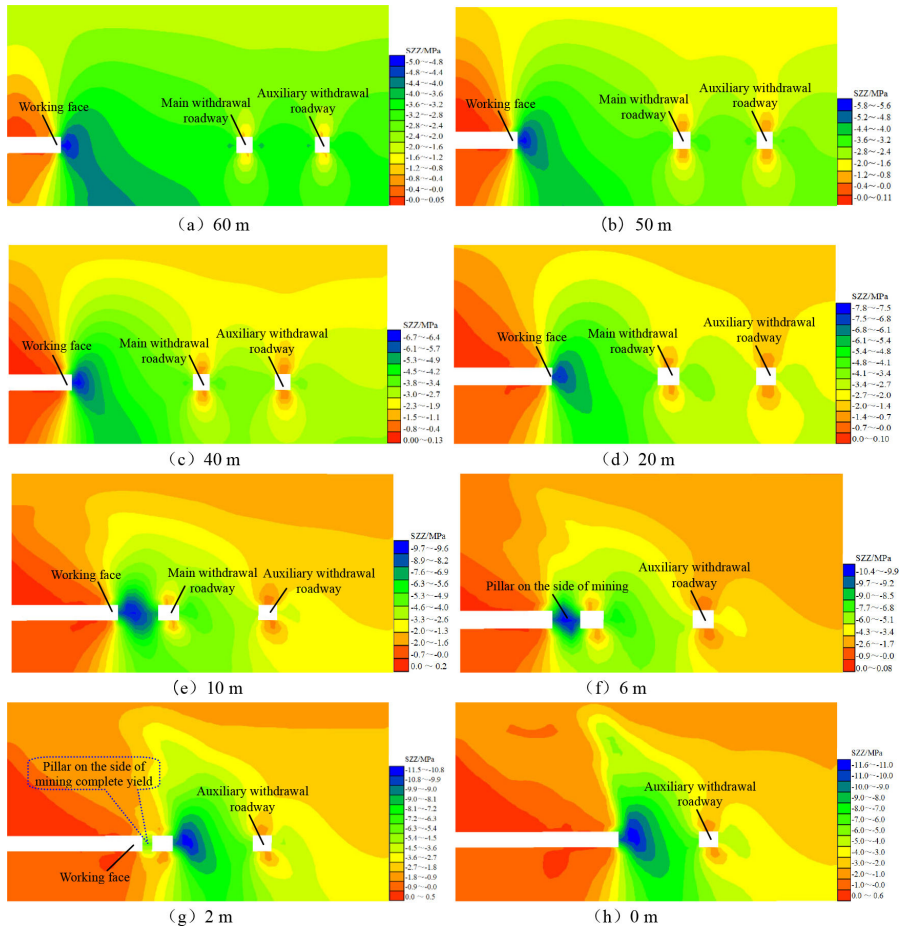


Figure 7: The stress evolution of the surrounding rock at distinct distances from the WF to the main withdrawal roadway.

roof weighting in the WF, and the simulated working resistance rapidly increased to 20,300 kN.

*3.2.3. Front Abutment Pressure.* Based on the gathered values from the floor CL-YB-114WX pressure sensors, the peak abutment pressure occurred about 10 m in front of the coal wall.

## 4. Superposition Effect of the Surrounding Rock Stress on the Last Mining Stage

*4.1. Design of FLAC$^{3D}$ Model.* The FLAC$^{3D}$ model was determined based on the geological and mining conditions of the 52304-WF, with dimensions of X = 300 m, Y = 270 m, and Z = 180 m, and adopted the Mohr–Coulomb criterion. The displacement boundary conditions were as follows: the upper boundary of the model was a free boundary, the lower boundary ($v_{Z}$ = 180 m) displacement was 0, the left and right boundary ($v_{X}$ = 0.300 m) displacements were 0, the front and rear boundary ($v_{Y}$ = 0.270 m) displacements were 0, the average unit weight of the overlying rock layer is 23 kN/m, and the gravity acceleration is 9.8 N/m$^2$. The mechanical parameters of the numerical calculation model are determined according to Table 1. Figure 6 shows the created model.

*4.2. Superposition Impact of the Front Abutment Pressure and Concentrated Stress of the Main Withdrawal Roadway.* The outcomes of the simulation dependent upon using the FLAC$^{3D}$ model suggest that Figure 7 illustrates the stress evolution of the surrounding rock at distinct distances from the main withdrawal roadway.

When the distance between the WF and the main withdrawal roadway decreased from 60 to 20 m, the corresponding front abutment pressure raised from 5.0 to 7.5 MPa, and the peak score was 10.0 m. These values are consistent with the experimental data. The concentrated stress of both sides of the primary withdrawal roadway was 4.0 MPa. At this time, the front abutment pressure and the concentrated stress of the main withdrawal roadway had not been superimposed.

It is observed that when the distance was 10 m, the front abutment pressure and the concentrated stress of the pillar overlap on the mining side. Moreover, the maximum front abutment pressure and the concentrated stress of the pillar on the side of mining increased to 9.7 and 8.5 MPa, respectively.

When the distance was 6 m, the front abutment pressure and the concentrated stress of the pillar on the side mining were completely superimposed. Furthermore, the asymmetrical distribution of concentrated stress appeared on both sides of the main withdrawal roadway. Under this circumstance, the concentrated stress of the coal pillar on the side of the mining was 10.0 MPa, which was 2.5 times of normal case. The mining-induced stress had a significant impact on the main withdrawal roadway.

When the distance was 2.0 m, the front abutment pressure of the WF was transferred to the coal pillar wall of the main withdrawal roadway, the peak stress reached 11.5 MPa, and the advance superposition of the stress field in the WF occurred. As the WF was joined with the main withdrawal roadway, the peak stress of the coal pillar wall was 11.6 MPa, indicating that the pillar on the mining side had completely collapsed as the WF approached the main withdrawal roadway.

The performed analyses reveal that once the WF approached the primary withdrawal roadway, the superposition effect of front abutment pressure and concentrated stress of the main withdrawal roadway was significant, which led to the complete collapse of the pillar on the side of the mining. As a result, the actual roof control distance of support and periodic weighting interval increased suddenly.

## 5. Structural Model of "Long Step Voussoir Beam" Under the "Static–Dynamic Load"

*5.1. Structural Model of "Long Step Voussoir Beam".* The physical simulation and numerical calculation revealed that as the WF approaches the primary withdrawal roadway, the superposition effect of front abutment pressure and concentrated stress of the main withdrawal roadway was significant, the coal pillar near the WF of the primary withdrawal roadway collapsed, and the main roof was broken ahead of the WF. Under this circumstance, the WF is subjected to the highest risk. Considering the impact of the main withdrawal roadway on the WF, both the roof control distance and periodic weighting interval of the WF increased. Consequently, the main roof presented a "long step voussoir beam" structure. Additionally, both "static loads" of the immediate roof and "dynamic loads" of the "long step voussoir beam" structure were increased, which were borne by hydraulic-powered support.

To further study the mechanism of strong mining pressure in the final mining stage, based on the basic conclusions obtained from physical simulation and numerical calculation, an established structural model of the "long step voussoir beam" under the superposition of "static and dynamic load" concerning the structural characteristics of the roof in the large mining height face, as shown in Figure 8.

Where $h_1$ and $h$ denote the thickness of the immediate and main roofs, respectively. Both $M$ and $N$ represent the key blocks of the main roof, and ω $\theta$ denotes the rotation angle of the blocks, respectively. Moreover, $b$ is the corresponding step height. A, C, and B represent the hinge points of key blocks. $\beta$ is the caving angle of the main roof. $T$ is the horizontal extrusion force. $R_M$ and $W$ are the dynamic and static loads borne by the support, respectively. $R_1$ is the residual reinforcing force of the pillar on the side of mining. $R_0$ is the reinforcement reaction of gob gangue to the key block N. $P$ is the working resistance of hydraulic-powered support.

*5.2. Structural Mechanical Analysis of "Long Step Voussoir Beam".* Referring to the stress analysis method of the "voussoir beam" structure [27], since the height of the corner extrusion surface of rock blocks is small, the height of the contact surface of the broken key block is negligible. Accordingly, the model of the key blocks when the WF approaches the main withdrawal roadway can be simplified as the following (Figure 9):

Where $l$ denotes the average periodic weighting interval before the WF through the main withdrawal roadway. $l_z$ is the increased length of the periodic weighting interval as the WF approaches the primary withdrawal roadway. $h$ is the main roof thickness. $P_1$ and $P_2$ are the weight of the key blocks $M$ and $N$ and the load that they bear, respectively. Furthermore, $Q_A$ and $Q_B$ represent the shear force at hinge joints A and B, respectively.

At point C, the key block $M$ is reinforced by the key block $N$, which is reinforced by the caved gangue in the gob. Therefore,

$$P_2 \approx R_0,\ Q_B \approx 0 \tag{1}$$

The equilibrium equation for the subsidence of the key block $N$ can be expressed in the form below:

$$\omega = m - (K_p - 1)h_1 \tag{2}$$

The equation for the step height of $M$ and $N$ key blocks is

$$b = \omega - klsin\theta \tag{3}$$

According to the balance characteristics of key blocks, the moment sum at point C in the key block $M$ is 0. This can be mathematically expressed as follows:

$$T\left[\frac{h\sin(\beta-\theta)}{\sin\beta} - \omega\right] + P_1\left[\frac{(l+l_Z)\cos\theta}{2} - \frac{b}{\tan(\beta-\theta)}\right] - Q_A\left[(l+l_Z)\cos\theta + \frac{h}{\sin\beta}\cos(\beta-\theta) - \frac{b}{\tan(\beta-\theta)}\right] \tag{4}$$

In addition, the resultant force along the vertical direction of key blocks is shown in equation (5).

$$Q_A + Q_B + R_0 - P_1 - P_2 = 0 \tag{5}$$

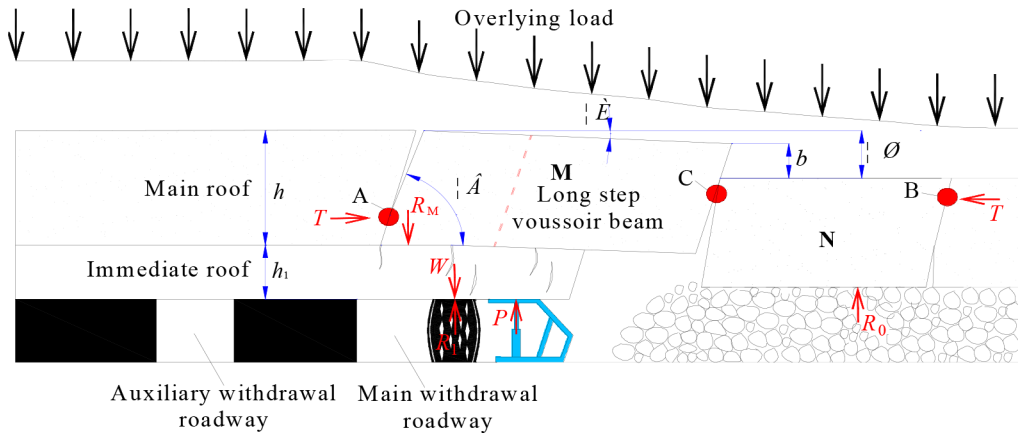


Figure 8: Structural model of "long step voussoir beam" of strong roof weighting in final mining.

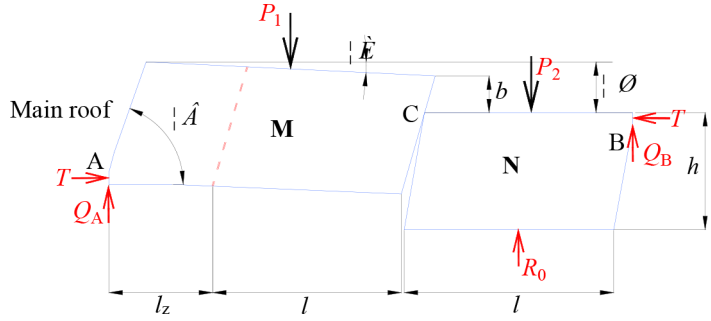


Figure 9: The mechanical analysis model of "long step voussoir beam."

Equations (1), (3), (4), and (5) can be combined to obtain the following expressions:

$$Q_A = P_1 \tag{6}$$

$$T = \frac{\frac{h}{\sin\beta}\cos(\beta-\theta)+\frac{l+l_Z}{2}\cos\theta}{\frac{h}{\sin\beta}\sin(\beta-\theta)-\omega}P_1 \tag{7}$$

Based on the "S–R" stability theory [28], this structure is prone to sliding instability unless the following inequality is met:

$$T\tan\phi + R_M \geq Q_A \tag{8}$$

$$R_M = P_1 - \frac{\frac{h}{\sin\beta}\cos(\beta-\theta)+\frac{l+l_Z}{2}\cos\theta}{\frac{h}{\sin\beta}\sin(\beta-\theta)-\omega}\tan\phi \tag{9}$$

$$P_1 = \left[1 - \frac{\frac{h}{\sin\beta}\cos(\beta-\theta)+\frac{l+l_Z}{2}\cos\theta}{\frac{h}{\sin\beta}\sin(\beta-\theta)-\omega}\tan\phi\right]P_1$$

where $P_1$ is the load borne by the key block $M$, which can be calculated from the following expression:

$$P_1 = ah\rho g(l+l_Z) + K_G a h_0\rho_0 g(l+l_Z) = a(l+l_Z)(h\rho g + K_G h_0\rho_o g) \tag{10}$$

According to the soil pressure theory of Terzaghi, the calculation formula of the load transfer coefficient is

$$K_G = \frac{l+l_Z}{2h_0\lambda\tan\phi_0} \tag{11}$$

The dynamic load carried by reinforcement due to the unsteadiness of the "long step voussoir beam" could be calculated by combining equations (9)–(11).

$$R_M = a\left[1 - \frac{\frac{h}{\sin\beta}\cos(\beta-\theta)+\frac{l+l_Z}{2}\cos\theta}{\frac{h}{\sin\beta}\sin(\beta-\theta)-\omega}\tan\phi\right]\left(h\rho g + \frac{l+l_Z}{2\lambda\tan\phi_0}\rho_0 g\right)(l+l_Z) \tag{12}$$

*5.3. Calculating the Support Working Resistance.* Figure 10 shows the computational model of the support working resistance when the large mining height face was nearly through the main withdrawal roadway.

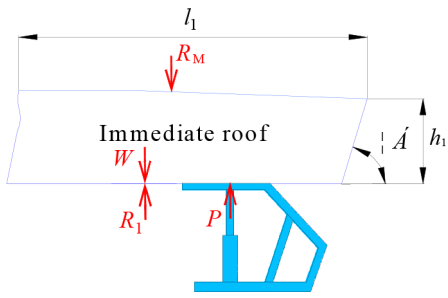


Figure 10: The calculation model of the support working resistance.

Where $l_1$ represents the actual roof control length of the hydraulic-powered support, and $\alpha$ denotes the caving angle of the immediate roof. The support working resistance of a large mining height face could be obtained through the following expression:

$$P = R_M + W - R_1 \tag{13}$$

where $R_M$, $W$, and $R_1$ depend on the width of the hydraulic-powered support.

The weight of the instant roof after coal seam mining is the static load carried by the support, which is directly proportional to its actual roof control distance. The static load can be calculated as follows:

$$W = a\left(l_1 + \frac{1}{2}h_1\cot\alpha\right)h_1\rho g \tag{14}$$

where $a$ is the width of the hydraulic-powered support.

Since the caving angle of the immediate roof is close to 90°, $\cot\alpha$ approaches zero. Therefore, equation (14) could be simplified in the form as follows:

$$W = al_1h_1\rho g \tag{15}$$

According to physical experiments and numerical calculations, as the WF approaches the primary withdrawal roadway, the coal pillar on the side of mining completely yields, and its residual support force can be ignored.

$$R_1 \approx 0 \tag{16}$$

The working resistance of hydraulic-powered support can be calculated by introducing equations (2), (12), (15), and (16) into equation (13).

$$P = a\left[1 - \frac{\frac{h}{\sin\beta}\cos(\beta-\theta) + \frac{l+l_Z}{2}\cos\theta}{\frac{h}{\sin\beta}\sin(\beta-\theta) - m + (K_P-1)h_1}\tan\phi\right] \left(h\rho g + \frac{l+l_Z}{2\lambda\tan\phi_0}\rho_0 g\right)(l+l_Z) + al_1h_1\rho g \tag{17}$$

where $l$ represents the initial average periodic weighting interval, $l_z$ denotes the increased length of the periodic weighting interval when the WF approaches the main withdrawal roadway, $a$ represents the width of hydraulic powered support, $K_p$ is the expansion ratio of the instant roof, $\tan\phi$ is friction coefficient of hinge point of the key block, $\rho g$ is the average bulk density of bedrock, $\lambda$ represents the lateral stress coefficient of load layer, $\tan\phi_0$ denotes the friction coefficient of load layer, and $\rho_0 g$ represents the average bulk density of load layer.

The rated working resistance of the support on the WF is defined by

$$P_e = \frac{P}{\mu} \tag{18}$$

where $\mu$ represents the reinforcement efficiency of hydraulic-powered support.

## 6. Case Analysis

According to physical simulation, numerical calculation, and mining conditions of 52304-WF, the following parameters were obtained.

$m$ = 6.0 m, $a$ = 2.05 m, $\rho g$ = 24.5 kN/m$^3$, $\rho_0 g$ = 23.4 kN/m$^3$, $\beta$ = 65.0°, $l$ = 20.7 m, $l_Z$ = 5.3 m, $\theta$ = 5.0°, $K_p$= 1.4, $\tan\phi$ = 0.5, $\tan\phi_0$ = 0.4, $\lambda$ = 1.0, $h$ = 20.4 m, $h_1$ = 5.2 m, $l_1$ = 11.5 m, and $\mu$ = 0.9.

*6.1. Calculation of Rational Support Working Resistance without the Main Withdrawal Roadway Influence.* In the stage when the WF was not impacted by the main withdrawal roadway, the length of the key block $N$ was approximately equal to that of the key block $M$, so $l_Z$ = 0, and the roof control distance of support was 4.5 m. Introducing these values into equations (17) and (18) yields the rated working resistance of the support in the stage of 52304-WF not affected by the main withdrawal roadway was 17,461.2 kN. The calculated value fits the field measurement and physical simulation, indicating that the theoretical calculation model is feasible.

*6.2. Calculation of Reasonable Support Working Resistance with the Main Withdrawal Roadway Influence.* When the WF approached the main withdrawal roadway, the actual roof control distance of support increased to 11.5 m (i.e., 2.56 times the normal state) and the periodic weighting interval increased to 26.0 m (i.e., 1.26 times the normal state).

Introducing parameters into equations (17) and (18) indicates that the rational working resistance of the hydraulic support as the WF approached the main withdrawal roadway was 19,757.5 kN. However, the rated working resistance of the support used on location was 16,800 kN. Concluded that when the WF approaches the primary withdrawal roadway, the roof fall and the support

crush mainly originate from the small working resistance of the hydraulic-powered support.

## 7. Conclusions

(1) According to the physical simulation, the main roof fall of 52,304 large-height mining face without the primary withdrawal roadway influence forms a "step voussoir beam" structure, the average caving angle and the rotation angle of the primary roof key block are 65° and 5°, respectively. Before the influence of the main withdrawal roadway, the mean periodic weighting interval is 20.7 m, and the mean support working resistance is 17,540 kN.

(2) The superposition effect of the front abutment pressure of the WF and the concentrated stress of the primary withdrawal roadway leads to the pillar completely collapsed. Meanwhile, the main roof caved ahead of the WF, forming a "long step voussoir beam" structure. As a result, the actual roof control distance of the support is 2.56 times, and the periodic weighting interval is 1.26 times the normal state. Additionally, increasing the roof control distance of support increases "static loads" of the immediate roof, and increasing the periodic weighting interval of the WF increases "dynamic loads" of the long step voussoir beam, both of which are borne by hydraulic-powered support.

(3) Based on those results, the structural model of the "long step voussoir beam" under the superposition of "static and dynamic load" is established, and an expression was derived to obtain the rational working resistance of the hydraulic-powered support as the WF approaches the main withdrawal roadway. Finally, the mechanism of roof fall and support crushing is revealed as the WF approaches the main withdrawal roadway. This article is expected to provide a guideline for the safe withdrawal of the large-height mining faces under similar conditions.

## Data Availability

The main relevant data is included in the paper, and the corresponding author will provide other relevant data according to reasonable requirements.

## Conflicts of Interest

The authors declare that the publication of this paper has no conflict of interest.

## Acknowledgments

We thank the National Natural Science Foundation of China, the Natural Science Basic Research Program of Shaanxi, and the State Key Laboratory for Fine Exploration and Intelligent Development of Coal Resources for their support of this study. We thank the academic editors and anonymous reviewers for their kind suggestions and valuable comments.

This work was funded by the National Natural Science Foundation of China (grant numbers 52204154 and 52074211), the Natural Science Basic Research Program of Shaanxi (grant number 2022JM-300), and the State Key Laboratory for Fine Exploration and Intelligent Development of Coal Resources (grant number SKLCRSM22KF004).

## References

[1] C. Li, X. F. Guo, T. H. Huo, and R. Liu, "Coal pillar design of pre-excavated double equipment withdrawal channel and its surrounding rock stability control," *J. Huazhong Univ. of Sci. & Tech.(Natural Science Edition)*, vol. 49, no. 4, pp. 20–25, 2021.

[2] Q. Y. Xu, Q. G. Huang, and YM. Li, "Mine strata pressure behavior law of fully mechanized top coal caving mining face during terminal mining period in Buliangou mine," *Coal Science and Technology*, vol. 41, no. 6, pp. 33–36, 2013.

[3] X. Ma, J. Li, F. Q. Xue, and XQ. Zhang, "Mechanical model of roof rupture weighting and its application in terminal mining stage of fully mechanized caving face," *Mining Safety & Environmental Protection*, vol. 43, no. 6, pp. 45–49, 2016.

[4] H. L. Liu and YK. Guo, "Law of mine pressure during the end mining of super-long working face in shallow medium-thick coal seam," *Coal Engineering*, vol. 53, no. 3, pp. 6–10, 2021.

[5] F. F. Zheng, Z. G. Sun, S. G. Li, W. T. Ye, and W. Guo, "Yield mining theory and roof control technology at end-mining stage of fully-mechanized face," *Mining Safety &Amp; Environmental Protection*, vol. 42, no. 2, pp. 64–67, 2015.

[6] P. H. Han, C. Zhang, Z. P. Ren, X. He, and S. Jia, "The influence of advance speed on overburden movement characteristics in longwall coal mining: insight from theoretical analysis and physical simulation," *Journal of Geophysics and Engineering*, vol. 18, no. 1, pp. 163–176, 2021.

[7] X. Z. Wang, J. L. Xu, W. B. Zhu, and JF. Ju, "Influence of high mining velocity on periodic weighting during fully-mechanized mining in a shallow seam," *Journal Of China University of Mining&Technology*, vol. 41, 2012.

[8] X. Z. Wang, J. F. Ju, and JL. Xu, "Theory and applicable of yield mining at ending stage of fully-mechanized face in shallow seam at Shendong mine Area," *Journal of Mining & Safety Engineering*, vol. 29, no. 3, pp. 151–156, 2012.

[9] S. Yang, J. G. Ning, H. F. Shang, Q. Xu, P. Q. Qiu, and N. Jiang, "Isobaric principle and application of end-mining stage in shallow buried near-distance coal seam working face," *Safety in Coal Mines*, vol. 50, no. 11, pp. 149–153, 2019.

[10] Z. Yang, D. Xu, M. S. Gao, X. Q. Xue, and DX. Zhang, "Key technologies of mine pressure regulation in the final mining withdrawal of high-cutting super-long fully mechanized working face," *Coal engineering*, vol. 52, no. 8, pp. 77–83, 2020.

[11] S. Ma, G. M. Tao, and ZG. Shi, "Application of joint grouting reinforcement technology in the end mining project of large mining height working face," *Coal engineering*, vol. 51, no. 4, pp. 49–53, 2019.

[12] DY. Gao, "Technology of roof control during terminal mining of fully-mechanized coal face with 7 m high cutting height," *Coal Science and Technology*, vol. 42, no. 10, pp. 121–124, 2014.

[13] H. Yao and J. I. A. X., "Discussion on through pressure supports in super long fully-mechanized coal face in shallow buried seam," *Coal Science and Technology*, vol. 45, no. S2, pp. 77–81, 2017.

[14] J. F. Lou, F. Q. Gao, J. H. Yang, et al., "Characteristics of evolution of mining-induced stress field in the longwall panel: insights from physical modeling," *International Journal of Coal Science & Technology*, vol. 8, no. 5, pp. 938–955, 2021.

[15] S. C. Gu, B. N. Wang, P. L. Su, X. S. Chen, and W. Chao, "Determination method for roof fracture position in retracement channel based on measured stress," *Safety in Coal Mines*, vol. 48, no. 7, pp. 224–227, 2017.

[16] S. C. Gu, B. N. Wang, R. B. Huang, and YP. Miao, "Method for determining the load on and width of coal pillar at the recovery room end of fully-mechanized longwall mining," *Journal of China University of Mining&Technology*, vol. 44, no. 6, pp. 990–995, 2015.

[17] S. C. Gu, R. B. Huang, and JH. Li, "Mined coal pillars during the pressure adjustment prior to working face trans-fixion," *Journal of Mining & Safety Engineering*, vol. 34, no. 1, pp. 60–66, 2017.

[18] Z. Q. Wang, S. S. Wang, and Z. H. Su, "New technology of collaborative work between face mining and bracket withdrawal," *Coal Science and Technology*, vol. 49, no. 2, pp. 21–29, 2021.

[19] HW. Lv, "The mechanism of stability of pre-driven rooms and the practical techniques," *Journal of China Coal Society*, vol. 39, no. S1, pp. 50–56, 2014.

[20] C. Zhang, Y. X. Zhao, P. H. Han, and QS. Bai, "Coal pillar failure analysis and instability evaluation methods: a short review and prospect," *Engineering Failure Analysis*, vol. 138, 2022.

[21] C. Zhang, Y. X. Zhao, X. He, J. T. Guo, and YG. Yan, "Space-sky-surface integrated monitoring system for overburden migration regularity in shallow-buried high-intensity mining," *Bulletin of Engineering Geology and the Environment*, vol. 80, no. 2, pp. 1403–1417, 2021.

[22] Y. L. Li, R. S. Yang, S. Z. Fang, et al., "Failure analysis and control measures of deep roadway with composite roof: a case study," *International Journal of Coal Science & Technology*, vol. 9, no. 1, p. 2, 2022.

[23] R. Gao, T. J. Kuang, Y. Q. Zhang, W. Y. Zhang, and CY. Quan, "Controlling mine pressure by subjecting high-level hard rock strata to ground fracturing," *International Journal of Coal Science & Technology*, vol. 8, no. 6, pp. 1336–1350, 2021.

[24] Q. X. Huang, J. L. Zhou, L. T. Ma, and PF. Tang, "Double key strata structure analysis of large mining height longwall face in nearly shallow coal seam," *Journal of China Coal Society*, vol. 42, no. 10, pp. 2504–2510, 2017.

[25] Q. X. Huang and JL. Zhou, "Roof weighting behavior and roof structure of large mining height longwall face in shallow coal seam," *Journal of China Coal Society*, vol. 41, no. S2, pp. 279–286, 2016.

[26] Q. X. Huang, J. Xu, and JW. Du, "Determination of support setting load of large-mining-height longwall face in shallow coal seam," *Journal of Mining & Safety Engineering*, vol. 36, no. 3, pp. 491–496, 2019.

[27] QX. Huang, *Ground control in longwall mining of shallow coal seam*, Science Press, Beijing, 2018.

[28] M. G. Qian, D. L. Zhang, L. J. Li, L. X. Kang, and JL. Xu, "S-R" stability for the voussoir beam and its application," *Ground Pressure and Roof Control*, vol. 3, pp. 6–11, 1994.